

Extreme NiI/FeI abundance ratio in the coma of the interstellar comet 3I/ATLAS*

Damien Hutsemékers¹, Jean Manfroid¹, Emmanuël Jehin¹, Cyrielle Opitom², Michele Bannister³, Juan Pablo Carvajal⁴, Rosemary Dorsey⁵, K Aravind¹, Baltasar Luco⁴, Brian Murphy², Thomas H. Puzia⁴, Rohan Rahatgaonkar⁴

¹ Institut d’Astrophysique et de Géophysique, Université de Liège, Allée du 6 Août 19c, 4000 Liège, Belgium

² Institute for Astronomy, University of Edinburgh, Royal Observatory, Edinburgh EH9 3HJ, United Kingdom

³ School of Physical and Chemical Sciences - Te Kura Matū, University of Canterbury, Private Bag 4800, Christchurch 8140, New Zealand

⁴ Institute of Astrophysics, Pontificia Universidad Católica de Chile, Av. Vicuña Mackenna 4860, 7820436 Macul, Santiago, Chile

⁵ Department of Physics, University of Helsinki, P.O. Box 64, 00014 Helsinki, Finland

Received ; accepted:

ABSTRACT

Emission lines of FeI and NiI are commonly found in the coma of solar system comets, even at large heliocentric distances. These atoms are most likely released from the surface of the comet’s nucleus or from a short-lived parent. The presence of these lines in cometary spectra is unexpected because the surface blackbody equilibrium temperature is too low to allow the sublimation of refractory minerals containing these metals. These lines were also found in the interstellar comet 2I/Borisov which has a NiI/FeI abundance ratio similar to that observed in solar system comets. On average, this ratio is one order of magnitude higher than the solar Ni/Fe abundance ratio. Here, we report observations of the new interstellar comet 3I/ATLAS, which were carried out with the ESO Very Large Telescope equipped with the UVES spectrograph. Spectra were obtained at six epochs, at heliocentric distances ranging from 3.14 to 2.14 au. NiI was detected at all epochs. FeI was only detected at heliocentric distances smaller than 2.64 au. We estimated the NiI and FeI production rates by comparing the observed line intensities with those produced by a fluorescence model. Comet 3I exhibits a high production rate of NiI atoms as well as a high NiI/FeI ratio, making it exceptional when compared to solar system comets and 2I/Borisov. Additionally, we found that the NiI/FeI ratio decreases rapidly with decreasing heliocentric distance, suggesting that comet 3I could soon become indistinguishable from solar system comets in this respect. We interpreted these observations assuming that the NiI and FeI atoms were released through the sublimation of Ni(CO)₄ and Fe(CO)₅ carbonyls, which supports the presence of these species in the cometary material.

Key words. Comets: general

1. Introduction

Numerous FeI and NiI emission lines have been identified in the spectra of about 20 solar system comets observed in the last two decades at heliocentric distances (r_h) ranging from 0.68 to 3.25 au (Manfroid et al. 2021; Hutsemékers et al. 2021; Hmidouch et al. 2025). The presence of these lines in cometary spectra at such distances from the Sun was unexpected because the surface blackbody equilibrium temperature is too low to allow the sublimation of silicate and sulfide minerals containing the metals. Furthermore, the mean abundance ratio NiI/FeI was found to be one order of magnitude higher than the solar ratio, and higher than the ratios estimated in the dust of 1P/Halley (Jessberger et al. 1988) and in the coma of the Sun-grazing comet Ikeya-Seki (Manfroid et al. 2021). Manfroid et al. (2021) advanced several mechanisms to explain these observations, in particular superheating of Ni-rich sulfides, possibly located in nanoparticles, and sublimation of organometallic complexes, such as carbonyls (see also Bromley et al. 2021 and Rahatgaonkar et al. 2025).

Interstellar comets, with potentially different chemical compositions, offer a unique opportunity to better understand the ori-

gin of the NiI and FeI atoms observed in cometary comae. FeI and NiI were found in the interstellar comet 2I/Borisov (Guzik & Drahus 2021; Opitom et al. 2021) with a NiI/FeI abundance ratio similar to the solar system comets. NiI was recently found in the interstellar comet 3I/ATLAS at a heliocentric distance of 3.88 au, before the onset of CN and FeI (Rahatgaonkar et al. 2025). This could support an unusual composition of comet 3I, as suggested by the very high CO₂/H₂O abundance ratio found by Cordiner et al. (2025).

In this work, we report the first detection of FeI emission lines in the coma of comet 3I/ATLAS at a heliocentric distance of 2.64 au. We measured the NiI/FeI abundance ratio at different heliocentric distances and compared it to the ratio observed in solar system comets and comet 2I/Borisov to determine whether comet 3I is unique.

2. Observations, data reduction, and measurements

Observations were carried out with the Very Large Telescope (VLT) at the European Southern Observatory (ESO), equipped with the UV-Visual Echelle Spectrograph(UVES¹). The standard settings 346+580 (dichroic 1), 390+580 (dichroic 1), and

* Based on observations made with the ESO Very Large Telescope at the Paranal Observatory under programs 115.C-0282 and 115.C-2317.

¹ UVES User Manual, VLT-MAN-ESO-13200-1825, <https://www.eso.org/sci/facilities/paranal/instruments/instruments.html>

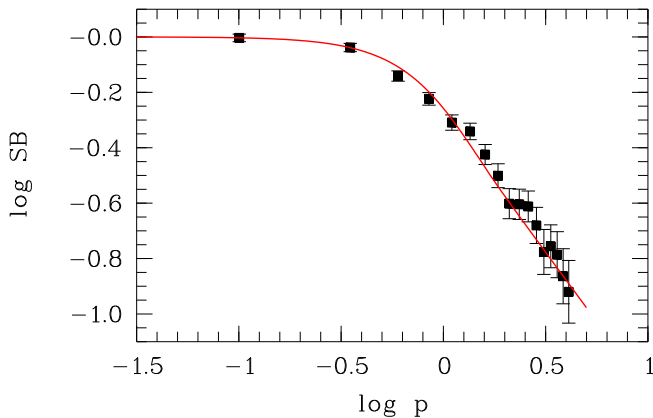


Fig. 1. Spatial profile of the brightest NiI line ($\lambda 3458\text{\AA}$) observed with UVES on September 4. The measured surface brightness (SB; normalized to one at the photocenter) is plotted as a function of the projected nucleocentric distance p in arcsec. The red line represents $\text{SB} \propto p^{-1}$ convolved with a $1.5''$ FWHM Gaussian to account for the seeing and tracking imperfections.

437+860 (dichroic 2) were used. The blue settings centered at 346 nm, 390 nm and 437 nm cover the spectral ranges 3030–3880 \AA , 3260–4540 \AA , and 3730–4990 \AA , respectively. A non-standard setting centered at 348 nm, corresponding to the spectral range 3100–3900 \AA , was also used to simultaneously cover the regions containing the OH and CN bands. Most of the time, a $1.8''$ -wide slit was used, delivering a resolving power of about 35000. The observing circumstances are summarized in Table A.1.

Raw frames were first processed to remove cosmic ray hits using the python implementation of the “lacosmic” package (van Dokkum 2001; van Dokkum et al. 2012). The data were reduced with the UVES pipeline² to obtain wavelength and flux calibrated two-dimensional spectra. One-dimensional spectra were then extracted by integrating over the slit length (Table A.2), using custom procedures. The scattered spectrum of the Sun (dust, twilight) was removed as described in Manfroid et al. (2009).

The intensities of unblended FeI and NiI emission lines were measured in the different spectra and compared to the intensities computed with a dedicated fluorescence model to derive FeI and NiI column densities. The procedure is described in detail in Manfroid et al. (2021). To compute the production rates from the column densities, we assume that the emission line surface brightness decreases as p^{-1} , where p is the projected nucleocentric distance, as observed in solar system comets (Manfroid et al. 2021; Hutsemékers et al. 2021), and in 3I itself (Fig. 1 and Sect. 3). The resulting production rates and abundance ratios are given in Table A.2, together with the number of lines used in the analysis.

The production rates of OH, CN, and C₂ were also estimated, using the OH(0-0) band at 3090 \AA , the CN(0-0) band at 3870 \AA , and the C₂ band at 5140 \AA . The rates were derived using the fluorescence efficiencies and Haser scalelengths from Schleicher & A'Hearn (1988), Cochran & Schleicher (1993), A'Hearn et al. (1995), and Schleicher (2010), with a parent and daughter velocity of $0.85 r_h^{-0.5} \text{ km s}^{-1}$ (Cochran & Schleicher 1993). These production rates are given in Table A.3.

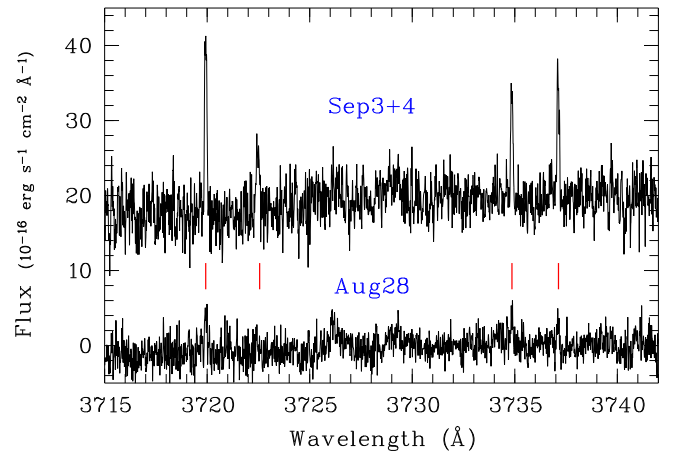


Fig. 2. Continuum-subtracted spectra of comet 3I obtained on August 28 and September 3+4. Three narrow FeI lines are detected on August 28 in this spectral range, FeI $\lambda 3719.93\text{\AA}$ being the brightest iron line detected in our spectra. On the average spectrum obtained in September 3+4 (shifted vertically for clarity), the FeI lines are brighter, and four of them are detected. Broad emission features due to background [OII] emission at 3727\AA and 3729\AA are also observed.

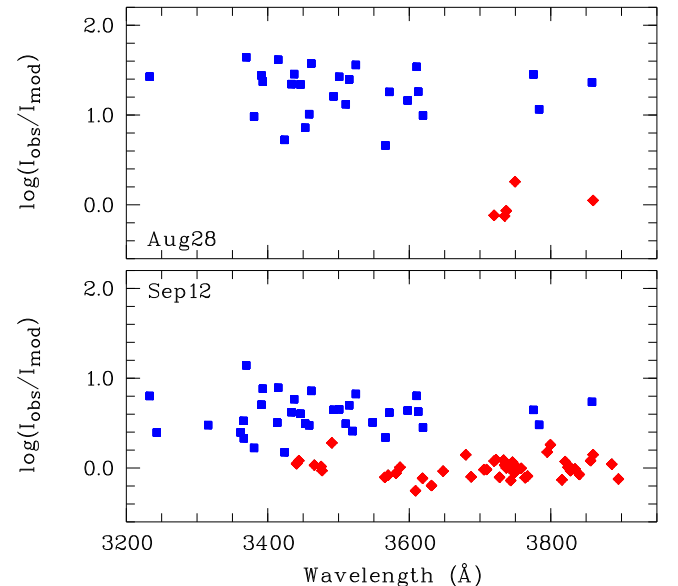


Fig. 3. The ratio $\log_{10}(I_{\text{obs}}/I_{\text{mod}})$ for the FeI (red diamonds) and NiI (blue squares) lines observed in comet 3I on August 28 (top) and September 12 (bottom). I_{obs} represents the observed line intensities and I_{mod} the intensities computed with the fluorescence model. $I_{\text{obs}}/I_{\text{mod}}$ is proportional to the column density of the atoms (see Manfroid et al. 2021, for details). The separation between the mean values computed for NiI and FeI gives the NiI/FeI abundance ratio. The ratios have been shifted on the y-axis so that the mean value of $\log_{10}(I_{\text{obs}}/I_{\text{mod}})$ is zero for FeI.

3. Analysis and results

One important characteristic of the FeI and NiI emission lines is their short spatial extent. In spectra obtained for comets 103P/Hartley2 and 46P at geocentric distances of 0.17 and 0.09 au, respectively, the surface brightness was found to be inversely proportional to the projected distance to the nucleus (Manfroid et al. 2021; Hutsemékers et al. 2021). Such a spatial profile indicates that the FeI and NiI atoms originate at nucleocentric distances smaller than about 50 km, either ejected from the surface

² UVES Pipeline User Manual, VLT-MAN-ESO-19500-2965, <https://www.eso.org/sci/software.html>

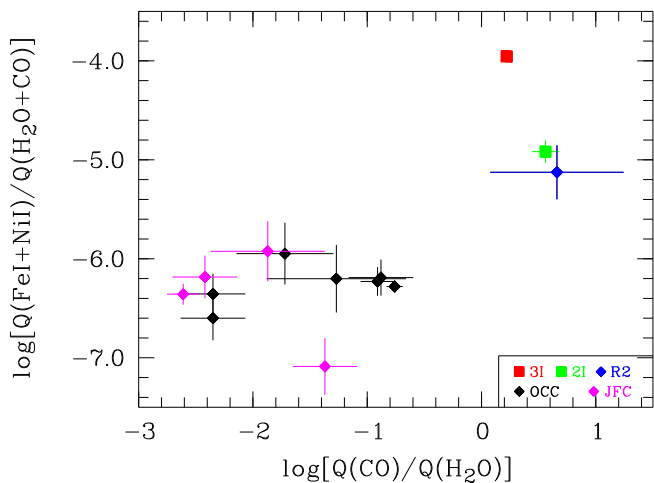


Fig. 4. Production rate ratio $Q(\text{FeI}+\text{NiI})/Q(\text{H}_2\text{O}+\text{CO})$ versus $Q(\text{CO})/Q(\text{H}_2\text{O})$ for interstellar and solar system comets. The CO and H_2O production rates of comet 3I are from Cordiner et al. (2025), when the comet was at 3.32 au. The CO and H_2O production rates of the other comets are from the compilation of Manfroid et al. (2021). The value of $Q(\text{FeI}+\text{NiI}) = Q(\text{NiI})$ which was considered for comet 3I is taken when the comet was at 3.14 au (August 12, see Table A.2).

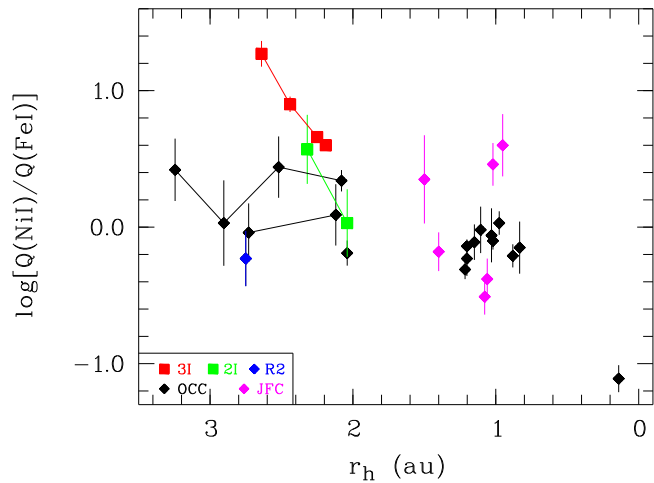


Fig. 5. $Q(\text{NiI})/Q(\text{FeI})$ as a function of the heliocentric distance r_h for interstellar and solar system comets. The measurements obtained at different heliocentric distances are not averaged and shown individually for comets 3I (4 values, pre-perihelion), 2I/Borisov (2 values, post-perihelion), C/2001 P1 (4 values, pre-perihelion), and C/2017 K2 (2 values, pre-perihelion). The comet with the smallest $Q(\text{NiI})/Q(\text{FeI})$ ratio is C/1965 S1 (Ikeya-Seki) observed at 0.14 au from the Sun. The solar Ni/Fe abundance ratio is equal, in logarithm, to -1.25 ± 0.04 (Asplund et al. 2009).

of the nucleus, or released from a short-lived parent. As shown in Fig. 1, a similar profile is observed for comet 3I.

While NiI lines were observed in the spectra obtained before August 28 and detected as far as 3.88 au (Rahatgaonkar et al. 2025, see also Table A.2), FeI lines were only detected in the spectra obtained on August 28 and after that date, when the comet was at $r_h \leq 2.64$ au. Some of the brightest FeI lines are shown in Fig. 2. After August 28, the lines steadily intensified, and new ones emerged until our final observations in mid-September (Figs. B.1 and B.2). The comparison of observed and computed line intensities is shown in Fig. 3, for two epochs. Although there is clearly some dispersion between the individual

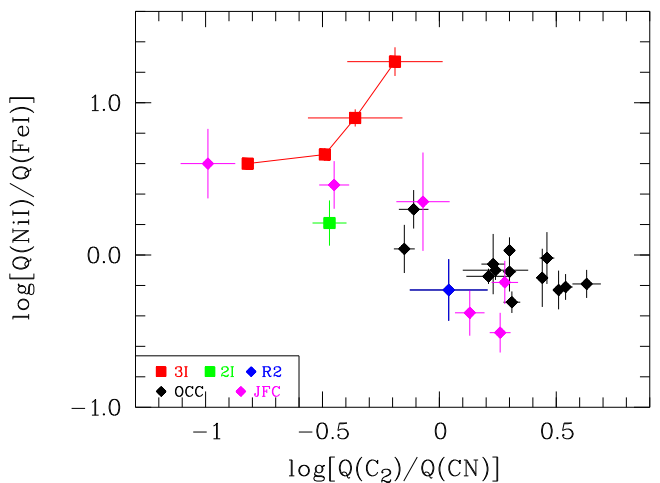


Fig. 6. $Q(\text{NiI})/Q(\text{FeI})$ as a function of the production rate ratio $Q(\text{C}_2)/Q(\text{CN})$.

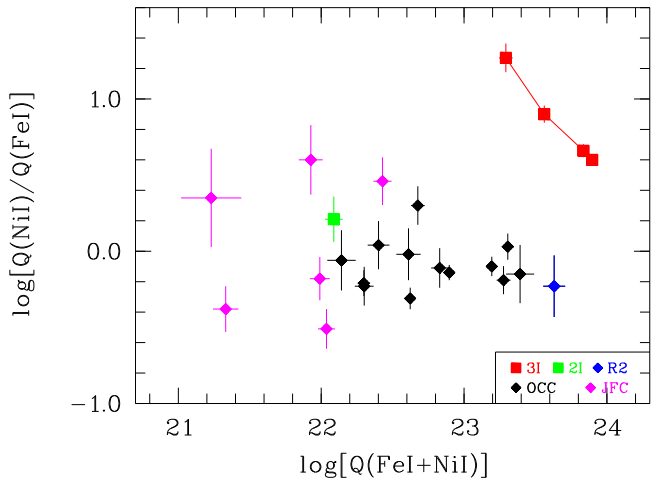


Fig. 7. $Q(\text{NiI})/Q(\text{FeI})$ as a function of the total production rate $Q(\text{FeI}+\text{NiI})$.

measurements, the average of the intensity ratios is well defined for both atomic species at the different epochs. The difference of the average values (in logarithm) gives the NiI/FeI abundance ratio (in logarithm), which is clearly higher on August 28 than on September 12 (Table A.2).

We compared the NiI and FeI production rates and the NiI/FeI abundance ratio measured in comet 3I to the same quantities evaluated in other comets (see Figs. 4-7). The NiI and FeI production rates were measured in approximately 20 comets based on UVES observations, except for comet C/1996 B2 (Hyakutake). The data are taken from Manfroid et al. (2021) and Hutsemékers et al. (2021), as are the production rates of C_2 and CN. These data include those obtained for the interstellar comet 2I/Borisov (Opitom et al. 2021). We also added the data of C/2017 K2 which was recently investigated by Hmidaoui et al. (2025). Unless otherwise stated, when more than one measurement is available for a given comet, we used the simple average, with errors computed from the individual measurements. For comet 3I, however, we show the individual measurements separately. Solar-system comets were classified into two broad categories: Jupiter-family comets (JFCs) and Oort-cloud comets (OCCs). For subgroup definitions and the identification of the individual comets in the plots, we refer to Manfroid et al. (2021)

and Hutsemékers et al. (2021). In the plots, we emphasized the measurements of the interstellar comet 2I/Borisov and of the unusual N₂-rich solar system comet C/2016 R2 (Opitom et al. 2019).

Figure 4 shows the ratio of Q(FeI+NiI) to Q(H₂O+CO) as a function of the ratio of Q(CO) to Q(H₂O), for the comets in the sample studied so far. Comets 3I, 2I/Borisov, and C/2016 R2, with their high CO/H₂O abundance ratios, are clearly distinct from the other comets. The observed correlation indicates that the release of NiI and FeI atoms begins before H₂O sublimates, when the comets are still very cold and their activity likely driven by the more volatile CO and CO₂. Figs. 5 through 7 show the production rate ratio Q(NiI)/Q(FeI) as a function of various quantities. In all these plots, comet 3I shows extreme properties, while comets 2I/Borisov and C/2016 R2 follow the global trends. Fig. 5 shows Q(NiI)/Q(FeI) as a function of the heliocentric distance. No correlation was found between Q(NiI)/Q(FeI) and r_h for the solar system comets (Manfroid et al. 2021). For some of them, Q(NiI)/Q(FeI) was measured at different heliocentric distances, and was found to be constant within the error bars. However, comet 3I breaks the rules by showing an extremely high Q(NiI)/Q(FeI) ratio at $r_h \approx 2.64$ au, and a rapid decrease with decreasing r_h . After two weeks, its value becomes compatible with that of the other solar system comets. In fact, we cannot exclude the possibility that some other comets exhibited the same behavior but they were simply not observed early enough with a sufficient signal to noise ratio.

A similar behavior is seen in Fig. 6, which shows the correlation found between Q(NiI)/Q(FeI) and Q(C₂)/Q(CN) (Hutsemékers et al. 2021): the Q(NiI)/Q(FeI) ratio of comet 3I measured in the first epochs is clearly higher than that of the other comets, but it rapidly decreases to align with them. Comet 3I appears as a C₂-depleted comets at all epochs, according to the criteria defined by Bair & Schleicher (2025) based on a large sample of solar-system comets. Although the errors are large for the first two epochs, Q(C₂)/Q(CN) seems to decrease with decreasing heliocentric distance, which is quite unusual; in most solar system comets, Q(C₂)/Q(CN) can slightly decrease but with increasing heliocentric distance, which is an artifact produced by the oversimplified Haser model used when deriving the C₂ production rates (Bair & Schleicher 2025).

In Fig. 7, comet 3I shows its most extreme behavior. While some solar system comets show either a NiI+FeI production rate or a NiI/FeI abundance ratio as large as those measured in comet 3I, comet 3I is characterized by both a high production rate of NiI atoms and a high Q(NiI)/Q(FeI) ratio.

4. Discussion and conclusions

The expected blackbody equilibrium temperature of the cometary surface is approximately $T \approx 280 r_h^{-1/2}$ K, where r_h is in au (Manfroid et al. 2021; Guzik & Drahus 2021; Puzia et al. 2025). At the distances at which the comets are observed, this temperature is far too low to vaporize silicate, sulfide, and metallic grains that contain NiI and FeI atoms. Therefore, the presence of NiI and FeI atoms in the cometary coma is extremely puzzling. Several hypotheses have been proposed to explain the presence of the NiI and FeI atoms at low surface temperatures as well as the high NiI/FeI abundance ratio, much higher than the solar system value. These scenarios were first presented by Manfroid et al. (2021), and discussed further by Bromley et al. (2021) and Rahatgaonkar et al. (2025). In particular, Manfroid et al. (2021) proposed that the NiI and FeI atoms could be released from Ni(CO)₄ and Fe(CO)₅ carbonyls, which are charac-

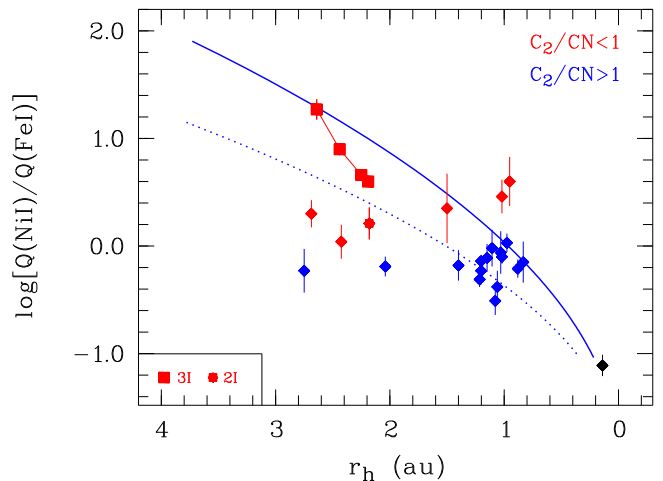


Fig. 8. Q(NiI)/Q(FeI) as a function of the heliocentric distance for interstellar and solar system comets. The comets with $Q(C_2)/Q(CN) < 1$ are represented in red, while comets with $Q(C_2)/Q(CN) > 1$ are represented in blue. C/1965 S1(Ikeya-Seki) (in black) has no $Q(C_2)/Q(CN)$ measurement. The curves represent the ratio of the sublimation rates of the Ni(CO)₄ and Fe(CO)₅ carbonyls (see text and Manfroid et al. 2021), assuming either $r_h = (280/T)^2$ (solid line) or $r_h = (350/T)^2$ (dotted line).

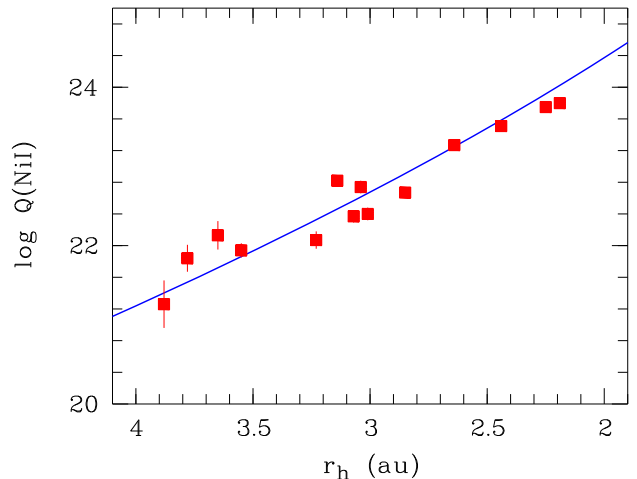


Fig. 9. Q(NiI) in comet 3I as a function of the heliocentric distance. The data are from this work and Rahatgaonkar et al. (2025). The curve represents the sublimation rate of the Ni(CO)₄ carbonyl (Manfroid et al. 2021), assuming $r_h = (280/T)^2$. The sublimation rate is computed in molecules m⁻² s⁻¹, and shifted vertically by 0.1dex to fit the observed production rates (in molecules s⁻¹). Thus, this shift corresponds to a very small effective emitting area of about 1.3 m², as could be expected for a minor species.

terized by very low sublimation temperatures. The lower sublimation temperature of Ni(CO)₄ with respect to Fe(CO)₅ could also explain the high NiI/FeI ratios observed at low surface temperatures. The carbonyl scenario, although appealing, predicts a Ni/Fe ratio that strongly depends on the temperature and thus on the heliocentric distance. Unfortunately, such a dependence was not observed in the sample of solar system comets studied by Manfroid et al. (2021).

On the contrary, comet 3I exhibits a net variation in its NiI/FeI abundance ratio as a function of the heliocentric distance (Fig. 5). Fig. 8 shows the ratio of the sublimation rates of Ni(CO)₄ and Fe(CO)₅ computed as a function of r_h , together with the measured NiI/FeI abundance ratios. The sublimation

rates were computed as a function of the temperature as done in Manfroid et al. (2021), and then as a function of r_h using the relation $T = 280 r_h^{-1/2}$. Finally, the ratio of the sublimation rates was corrected for the solar system Ni/Fe abundance ratio, $\log_{10}(\text{Ni/Fe}) = -1.25$ (Asplund et al. 2009). Bromley et al. (2021) showed that the photodissociation of $\text{Ni}(\text{CO})_4$ and $\text{Fe}(\text{CO})_5$ into NiI and FeI occurs at very similar rates for both carbonyls and at distances consistent with the observed spatial distributions of the atoms, making comparisons between atomic production rates and carbonyl sublimation rates meaningful. Remarkably, the carbonyl sublimation ratio reproduces the NiI/FeI ratio observed in several comets, but not all. In particular, it reproduces the ratio measured in comet 3I at the onset of FeI at $r_h \approx 2.64$ au. However, the rapid decrease of NiI/FeI with r_h in comet 3I does not follow the theoretical curve (Fig. 8). The ratio of the carbonyl sublimation rates therefore appears as an upper limit to the observed NiI/FeI ratios. Rahatgaonkar et al. (2025) recorded the emergence of NiI, and found that its production rate changes with the heliocentric distance much faster than expected from purely radiative processes. As shown in Fig. 9, this steep dependence can be reproduced assuming that the NiI production rate is essentially controlled by the $\text{Ni}(\text{CO})_4$ carbonyl sublimation rate. The behavior of comet 3I suggests that carbonyl sublimation begins very early, well before the release of water and dust. At this stage, the surface temperature of the nucleus is close to the black-body equilibrium temperature. As the comet approaches the Sun, more material is ejected, particularly dust, which can raise the temperature beyond the black-body equilibrium temperature, at least in localized regions (Prialnik et al. 2004; Groussin et al. 2013; Höfner et al. 2017). Since the carbonyl sublimation rate increases rapidly with the temperature, hot regions can dominate their sublimation, producing NiI and FeI atoms with a NiI/FeI abundance ratio lower than expected at the equilibrium temperature (see the dotted curve in Fig. 8). The absence of a net correlation between the NiI/FeI ratio and r_h for solar system comets may simply be due to the dispersion of their temperatures and surface properties at a given heliocentric distance. If this interpretation is correct, the NiI/FeI ratio could be used to estimate the temperature of a cometary nucleus, or subregions at its surface.

While this scenario provides a straightforward way to understand the behavior of NiI and FeI atoms in comets and supports the existence of carbonyls in cometary material, it is clear that there is more to the story, as the NiI/FeI ratio is also influenced by the carbon content, as demonstrated by the relationship between the NiI/FeI and C_2/CN ratios (Fig. 8; see also Fig. 6). As the C_2 depletion is primordial rather than evolutionary (Bair & Schleicher 2025), the NiI/FeI abundance ratio could also be a primordial property, at least in part. The possible link between the production of metal atoms and the abundance of carbon oxides (Fig. 4), suggests that when more CO or CO_2 molecules are available in the cometary material, more Ni and Fe could have been incorporated in carbonyls during the comet formation, so that more NiI and FeI atoms are finally produced when these carbonyls sublime. A better understanding of the formation of carbonyls in various chemical environments would be needed, in particular to see if an initial $\text{Ni}(\text{CO})_4 / \text{Fe}(\text{CO})_5$ asymmetry can already be produced during the comet formation, depending on the carbon content. Finally, it is worth to remember that other mechanisms, such as superheating of nanograins, could also contribute to the release of NiI and FeI atoms from refractory material, with a less extreme NiI/FeI ratio (see Manfroid et al. 2021). At the end, for Sun-grazing comets, complete vaporization of

refractory grains occurs, leading to a solar NiI/FeI abundance ratio.

In conclusion, comet 3I, which is a C_2 -depleted comet, exhibits extreme properties in the early phases of its activity with regard to the production rates and abundance ratios of NiI and FeI. The rapid changes with the heliocentric distance suggest that comet 3I could soon become indistinguishable from solar system comets with respect to the NiI/FeI ratio. Nevertheless, comet 3I remains exceptional compared to solar system comets due to its high, asymmetrical production rate of NiI and FeI (Fig. 7). Compared to comets in the solar system, comet 3I is either metal-rich, which could potentially constrain the predictions of Hopkins et al. (2025), or, more likely, it has enhanced metal production due to chemical anomalies, such as the very high $\text{CO}_2/\text{H}_2\text{O}$ abundance ratio (Cordiner et al. 2025).

Acknowledgements. DH and EJ are Research Directors at the F.R.S-FNRS. JM is honorary Research Director at the F.R.S-FNRS.

References

- A'Hearn, M. F., Millis, R. C., Schleicher, D. O., Osip, D. J., & Birch, P. V. 1995, *Icarus*, 118, 223
 Asplund, M., Grevesse, N., Sauval, A. J., & Scott, P. 2009, *ARA&A*, 47, 481
 Bair, A. N. & Schleicher, D. G. 2025, arXiv e-prints, arXiv:2509.05499
 Bromley, S. J., Neff, B., Loch, S. D., et al. 2021, *Planetary Science Journal*, 2, 228
 Cochran, A. L. & Schleicher, D. G. 1993, *Icarus*, 105, 235
 Cordiner, M. A., Roth, N. X., Kelley, M. S. P., et al. 2025, arXiv e-prints, arXiv:2508.18209
 Groussin, O., Sunshine, J. M., Feaga, L. M., et al. 2013, *Icarus*, 222, 580
 Guzik, P. & Drahus, M. 2021, *Nature*, 593, 375
 Hmidaouch, S., Jehin, E., Lippi, M., et al. 2025, arXiv e-prints, arXiv:2507.13451
 Höfner, S., Vincent, J. B., Blum, J., et al. 2017, *A&A*, 608, D
 Hopkins, M. J., Dorsey, R. C., Forbes, J. C., et al. 2025, *ApJ*, 990, L30
 Hutsemékers, D., Manfroid, J., Jehin, E., Opitom, C., & Moulane, Y. 2021, *A&A*, 652, L1
 Jessberger, E. K., Christoforidis, A., & Kissel, J. 1988, *Nature*, 332, 691
 Manfroid, J., Hutsemékers, D., & Jehin, E. 2021, *Nature*, 593, 372
 Manfroid, J., Jehin, E., Hutsemékers, D., et al. 2009, *A&A*, 503, 613
 Opitom, C., Hutsemékers, D., Jehin, E., et al. 2019, *A&A*, 624, A64
 Opitom, C., Jehin, E., Hutsemékers, D., et al. 2021, *A&A*, 650, L19
 Prialnik, D., Benkhoff, J., & Podolak, M. 2004, in *Comets II*, ed. M. C. Festou, H. U. Keller, & H. A. Weaver, 359
 Puzia, T. H., Rahatgaonkar, R., Carvajal, J. P., Nayak, P. K., & Luco, B. 2025, *ApJ*, 990, L27
 Rahatgaonkar, R., Carvajal, J. P., Puzia, T. H., et al. 2025, arXiv e-prints, arXiv:2508.18382
 Schleicher, D. G. 2010, *AJ*, 140, 973
 Schleicher, D. G. & A'Hearn, M. F. 1988, *ApJ*, 331, 1058
 van Dokkum, P. G. 2001, *PASP*, 113, 1420
 van Dokkum, P. G., Bloom, J., & Tewes, M. 2012, *Astrophysics Source Code Library*, ascl:1207.005

Appendix A: Tables

Table A.1. Observing circumstances.

Date yyyy-mm-dd	r_h au	\dot{r}_h km s $^{-1}$	Δ au	$\dot{\Delta}$ km s $^{-1}$	Settings	w_B/w_R "	h_B/h_R "
2025-08-12	3.14	-55.3	2.69	-15.4	346+580	1.8/0.6	9.5/11.5
2025-08-15	3.04	-54.9	2.66	-13.3	390+580	0.6/0.6	7.5/11.5
2025-08-28	2.64	-52.9	2.59	-6.6	348+580	1.8/0.6	9.5/11.5
2025-08-28	2.64	-52.9	2.59	-6.6	437+860	1.8/0.6	9.5/11.0
2025-09-03	2.46	-51.6	2.57	-4.8	348+580	1.8/1.2	9.5/11.5
2025-09-03	2.46	-51.6	2.57	-4.8	437+860	1.8/1.2	9.5/11.0
2025-09-04	2.43	-51.3	2.57	-4.6	348+580	1.8/1.2	9.5/11.5
2025-09-04	2.43	-51.3	2.57	-4.6	437+860	1.8/1.2	9.5/11.0
2025-09-10	2.25	-49.5	2.55	-3.7	348+580	1.8/1.2	9.5/11.5
2025-09-11	2.22	-49.2	2.55	-3.7	437+860	1.8/1.2	9.5/11.0
2025-09-12	2.19	-48.8	2.55	-3.6	348+580	1.8/1.2	9.5/11.5
2025-09-14	2.14	-48.1	2.54	-3.6	437+860	1.8/1.2	9.5/11.0

Notes. r_h and Δ are the heliocentric and geocentric distances of the comet. \dot{r}_h and $\dot{\Delta}$ are the corresponding velocities. w_B , w_R , h_B , and h_R refer to the blue/red slit width and height, respectively.

Table A.2. FeI and NiI production rates, and their ratio.

Date yyyy-mm-dd	n_{lines} FeI / NiI	$\log_{10} Q(\text{FeI})$ s $^{-1}$	$\log_{10} Q(\text{NiI})$ s $^{-1}$	$\log_{10} [Q(\text{NiI})/Q(\text{FeI})]$
2025-08-12	- / 20	< 21.83	22.82 ± 0.06	> 0.99
2025-08-15	- / 14	< 22.14	22.74 ± 0.08	> 0.60
2025-08-28	5 / 28	22.00 ± 0.08	23.27 ± 0.05	1.27 ± 0.10
2025-09-3/4	17 / 36	22.61 ± 0.04	23.51 ± 0.04	0.90 ± 0.06
2025-09-10	42 / 36	23.09 ± 0.03	23.75 ± 0.03	0.66 ± 0.04
2025-09-12	46 / 37	23.20 ± 0.02	23.80 ± 0.03	0.60 ± 0.04

Notes. The data obtained on Sept. 3 and 4 in very similar circumstances were averaged to increase the signal-to-noise ratio.

Table A.3. OH, CN, and C₂ production rates.

Date yyyy-mm-dd	$\log_{10} (\text{OH})$ s $^{-1}$	$\log_{10} Q(\text{CN})$ s $^{-1}$	$\log_{10} Q(\text{C}_2)$ s $^{-1}$
2025-08-12	-	24.0 ± 0.3	-
2025-08-15	-	24.35 ± 0.05	-
2025-08-28	26.37 ± 0.04	24.79 ± 0.04	24.6 ± 0.2
2025-09-3/4	26.59 ± 0.02	24.96 ± 0.03	24.6 ± 0.2
2025-09-10	27.05 ± 0.13	24.85 ± 0.01	24.36 ± 0.02
2025-09-11	-	25.16 ± 0.01	-
2025-09-12	27.15 ± 0.10	25.29 ± 0.01	24.47 ± 0.01
2025-09-14	-	25.26 ± 0.01	-

Notes. The data obtained on Sept. 3 and 4 in very similar circumstances were averaged to increase the signal-to-noise ratio.

Appendix B: Evolution of NiI and FeI emission lines

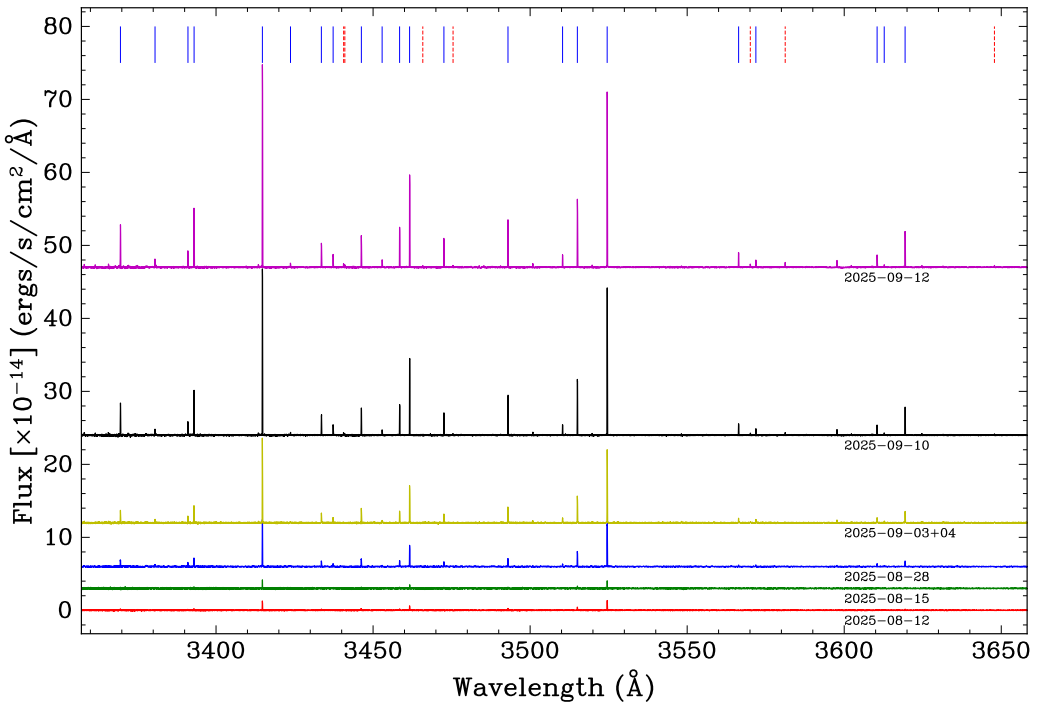


Fig. B.1. UVES blue, continuum-subtracted, spectra of comet 3I from August 12 to September 12. They show the evolution of the NiI (solid blue tickmarks) and FeI lines (dashed red tickmarks) in the spectral range 3360–3650 Å. The flux scale is identical for all spectra, which are shifted vertically for clarity.

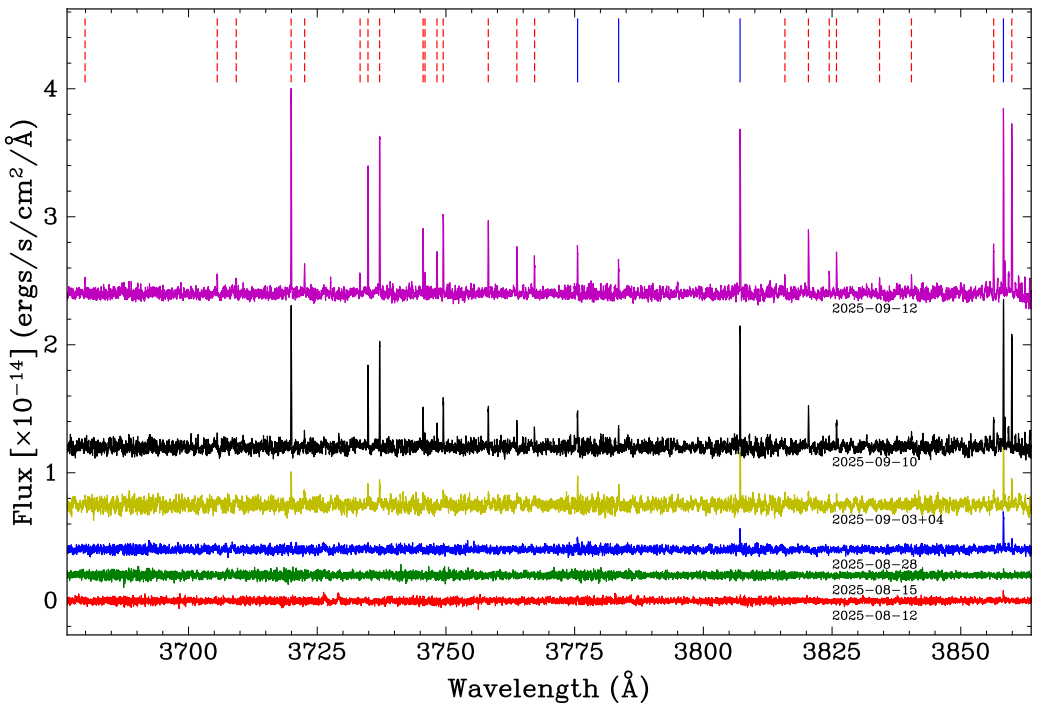


Fig. B.2. Same as Fig. B.1 for the 3680 – 3860 Å spectral range.